ARTICLE

Recent advances in oxidative allylic C–H functionalization *via* group IX-metal catalysis

Received 00th January 20xx, Accepted 00th January 20xx

DOI: 10.1039/x0xx00000x

Amaan M. Kazerouni, a Quincy A. McKoy a and Simon B. Blakey *a

Allylic substitution, pioneered by the work of Tsuji and Trost, has been an invaluable tool in the synthesis of complex molecules for decades. An attractive alternative to allylic substitution is the direct functionalization of allylic C-H bonds of unactivated alkenes, thereby avoiding the need for prefunctionalization. Significant early advances in allylic C-H functionalization were made using palladium catalysis. However, Pd-catalyzed reactions are generally limited to the functionalization of terminal olefins with stabilized nucleophiles. Insights from Li, Cossy, and Tanaka demonstrated the utility of RhCp $^{\times}$ catalysts for allylic functionalization. Since these initial reports, a number of key intermolecular Co-, Rh-, and Ircatalyzed allylic C-H functionalization reactions have been reported, offering significant complementarity to the Pd-catalyzed reactions. Herein, we report a summary of recent advances in intermolecular allylic C-H functionalization via group IX-metal π -allyl complexes. Mechanism-driven development of new catalysts is highlighted, and the potential for future developments is discussed.

Introduction

Transition metal-catalyzed functionalization of relatively inert C–H bonds to form carbon-carbon (C–C) or carbon-heteroatom (C–X) bonds has evolved from a mechanistic curiosity to an indispensable tool in the synthetic toolbox. The maturation of the field of C–H functionalization has had a dramatic effect in the streamlining of complex molecule synthesis in the context of atom-, step-, and redox-economy. Nonetheless, the vast opportunity presented by the concept of selective C–H functionalization in complex settings dictates that many challenges remain, in almost every facet of C–H functionalization research.

In this review, we will discuss recent advances in allylic C–H functionalization via group IX transition metal $\pi\text{-allyl}$ complexes. 9,10 These reactions are alluring alternatives to allylic substitution, $^{11-15}$ promising the possibility of using both simple feedstock olefins and complex natural products directly as substrates. However, to realize this promise, further advances in catalyst development addressing both reactivity and selectivity are required.

In 2005, White and coworkers reported a palladium catalyst system capable of catalytic generation of a Pd(π -allyl) complex which could be intercepted with a range carbon, oxygen, and nitrogen nucleophiles. While these early advances from White, Stahl, and others have established catalytic allylic C–H functionalization as an attractive alternative to traditional Tsuji-

Trost allylations, they are largely limited to terminal olefins and generally require the use of stabilized nucleophiles. In most cases, the formation of the linear functionalized products is observed (Figure 1A).

Since these early reports, allylic C–H functionalization has grown to include rhodium, iridium, and ruthenium catalysis, ^{29,30} further expanding the scope of olefin and nucleophile coupling partners compatible with these reactions. In this Feature Article, we summarize recent contributions to the field of Rhand Ir-catalyzed allylic C–H functionalization that have significantly expanded the scope and potential of these reactions (Figure 1B).

A. Pd-catalyzed Allylic C–H Functionalization of Terminal Olefins (White, Stahl, others)

B. Rh- and Ir-Catalyzed Allylic C-H Functionalization (This Feature Article)

Figure 1: Recent advances in allylic C-H functionalization

a. Department of Chemistry, Emory University, Atlanta, Georgia 30322, United States.

[†] Footnotes relating to the title and/or authors should appear here. Electronic Supplementary Information (ESI) available: [details of any supplementary information available should be included here]. See DOI: 10.1039/x0xx00000x

RhCp*-catalyzed oxidative allylic C-H functionalization using external oxidants

Until recently, allylic C-H functionalization via transition-metal $\pi\text{-allyl}$ complexes was dominated by palladium catalysis. 29,30 However, these reactions - the state of the art allylic C-H functionalization technology at the time - were largely limited to terminal olefins and stabilized nucleophiles. In 2011, Li and co-workers demonstrated that, in the presence of excess Cu(OAc)2, naphthalene 1 could undergo C-H olefination (to form product 2), followed by formal allylic C–H functionalization to form 3 as the major product (Figure 2A).31 At the time, it was unclear whether this step was taking place via a Rh(III)Cp*(πallyl) complex or through Wacker type amination and β-hydride elimination. The first systematic exploration of this area was disclosed in 2012, when Cossy and coworkers reported the Rh(III)Cp*-catalyzed intramolecular allylic C-H amination of alkenyl sulfonamides (Figure 2B).32 While the substrate scope consisted predominantly of terminal olefins, in one particularly

A. Rh-catalyzed intermolecular allylic C–H amination of an internal olefin (Li, 2011)

B. Rh-catalyzed intramolecular allylic C–H amination of an internal olefin (Cossy, 2012)

$$\begin{array}{c} \text{TsHN} \\ \text{H} \\ \text{H} \\ \text{H} \\ \text{Interpretal points of the properties of the$$

C. Stoichiometric formation and functionalization of RhCp $^{\text{E}}$ π -allyl complex (Tanaka, 2016)

D. Selectivity in π -allyl complex formation from an internal olefin (Tanaka, 2016)

Figure 2: Early insights in intramolecular RhCp*-catalyzed allylic C–H amination

intriguing example, the internal olefin **4** could be functionalized to form piperidine **5** and pyrrolidine **6** in a 1:1 ratio and 50% combined yield. The authors speculated that the reaction was proceeding through a Rh(III)Cp*(π -allyl) complex produced by allylic C–H activation on either side of the internal olefin, leading to the observed product distribution. These reports from Li and Cossy were the first examples of allylic C–H amination of internal olefins. Additionally, they diverged significantly from the Pd literature, by demonstrating that alkylamines activated by only one electron-withdrawing group were competent as nucleophiles, offering significant opportunity for further development.

In 2016, Tanaka and coworkers reported the stoichiometric formation of Rh(III)Cp^E(π -allyl) complex I and subsequent conversion to vinylpyrrolidine 8 upon treatment with an external oxidant (Figure 2C), providing experimental support for Cossy's hypothesis that the Rh(III)Cp*-catalyzed intramolecular allylic C–H amination was proceeding through a π -allyl intermediate.33 Complex I was also shown to be catalytically competent in the allylic C-H amination of 7 to directly form vinylpyrrolidine 8 (not shown), further supporting the intermediacy of a RhCp*(π -allyl) complex in this reaction. In the same report, the authors showed that formation of the thermodynamically more stable internal RhCp^E- $(\pi$ -allyl) complexes IIb and IIc was favored over the terminal complex IIa (Figure 2D). This result was particularly significant as it suggested that RhCp* complexes could potentially differentiate between similar allylic C-H bonds on unsymmetrical olefins, offering enticing potential for subtle selective reactions of internal olefins. These early discoveries from the Cossy and Tanaka groups suggested that the RhCp-based complexes could be competent catalysts for the intermolecular allylic C-H functionalization of internal olefins.

Rh(III)Cp*-catalyzed intermolecular allylic C-H amination

Armed with this insight, in 2017, we set out to develop a regioselective intermolecular allylic C–H amination of internal olefins (Figure 3).³⁴ In initial studies, focused on demonstrating the potential for efficient intermolecular reactions, 1,3-diphenylpropene (DPP) was successfully aminated with a variety of nitrogen nucleophiles. The expanded substrate compatibility of this reaction was exemplified in the use of alkyl (12a) and aryl (12b) tosylamides, monoprotected amines (12c–12f), and *N*-Cbz-glycine (12g) as the nitrogen nucleophile. This study

NHTs

Figure 3: RhCp*-catalyzed intermolecular allylic C–H amination of internal olefins (Blakey, 2017)

demonstrated for the first time that an amine of choice could be coupled in an intermolecular fashion with an olefin substrate. The study also demonstrated that differentially substituted 1,2-disubstituted olefins could be regioselectively aminated. An electronically diverse array of β -alkylstyrenes (10h-10n), including substrates with oxidatively sensitive heteroaromatics like thiophene ($\mathbf{10m}$) and indole ($\mathbf{10n}$), were all competent in the reaction. Notably, in all cases, the reaction was selective for the conjugated allylic amine products. In some cases, an allylic acetate side product was observed (always as a minor component). At longer reaction times and higher temperatures, product equilibration between the two regioisomers of the allylic amine and the allylic acetate was observed, with the product distribution funneling towards the conjugated allylic amine. This observation indicated that C-N and C-O bond formation was reversible under the reaction conditions.

In a 2019 follow-up study (Figure 4), the Jeganmohan group reported the IrCp*-catalyzed variant of this reaction and observed a similar trend in regioselectivity of styrenyl substrates for the conjugated products.³⁵ Additionally, they

Figure 4: Regioselectivity in IrCp*-catalyzed allylic C–H amination of unsymmetrical 1,3-diarylpropenes (Jeganmohan, 2019)

demonstrated that on an unsymmetrical aryl-aryl IrCp*(π -allyl) complex, the allylic amine product with the olefin in conjugation with the more electron-deficient aryl ring was favored.

Rh(III)Cp*-catalyzed allylic C-H etherification

The intermolecular formation of C-O bonds by allylic C-H functionalization remains an under-explored transformation, with previous examples being limited to the functionalization of terminal olefins or stabilized carboxylate nucleophiles.^{29,30} These reactions are challenging because the alcohol starting materials and ether products are particularly susceptible to oxidation under the oxidative conditions required for allylic Cfunctionalization. In 2018, we reported the first intermolecular allylic C-H etherification of internal olefins (Figure 5).36 The reaction was effective across an array of primary (17a-17c) and secondary (17d and 17e) alkyl alcohols. Important biologically active building blocks such as galactose (17f), morpholine (17g), and serine (17h) derivatives were effectively coupled. Strained ring substrates, that might be sensitive to the Lewis acid components of the reaction conditions, such as the 4-membered heterocycles oxetane (17i) and azetidine (17j) were tolerated. With stereogenic substrates (17e-17h), almost no diastereoselectivity was observed. As with the amination reaction, a range of β -alkylstyrene substrates could be converted to their corresponding allyl ethers, including ortho-substituted arenes (17k and 17l), as well as phenylalanine- (17m), estrone- (17n),

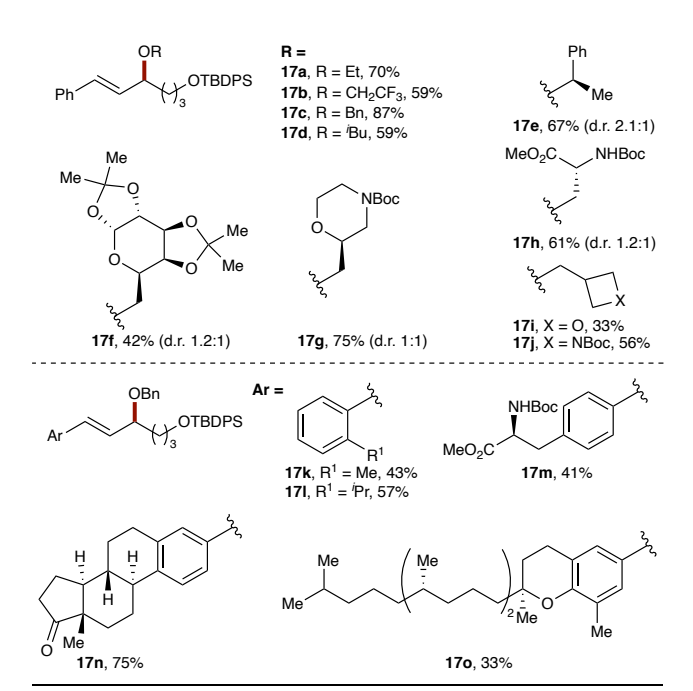


Figure 5: RhCp*-catalyzed intermolecular allylic C–H etherification of internal olefins (Blakey, 2018)

and tocopherol-derived **(170)** olefins. The regioselectivity of this system was consistent with that observed in the amination reaction, delivering the allyl ether with the olefin in conjugation with the aryl ring.

Rh(III)Cp*-catalyzed allylic C-H arylation

In 2018, Glorius and co-workers demonstrated that electron rich heteroaromatics could also be used as nucleophiles in these allylic C-H functionalization reactions (Figure 6).³⁷ The substrate scope consisted of a range of 5-substituted thiophenes (19a-19e) and furans (19f-19h) as well as other heterocycles such as benzofuran (19i), benzothiophene (19j), and N-methylindole (19k). 1,3,5-trimethoxybenzene was also a suitably electronrich nucleophile, providing the arylated product 19m, albeit in lower yield. On substrates that proceeded through unsymmetrical styrenyl π -allyl complexes (19n–19q), the reaction generally displayed good selectivity for the conjugated arylated products, consistent with the regiochemical outcome observed in our reports of allylic amination and etherification. Conversely, 4-octene was converted to a 1:1 mixture of regioisomeric allylic thiophenes 19s and 19s', consistent with the hypothesis that this reaction proceeded through a Rh(III)Cp*(π -allyl) intermediate complex.

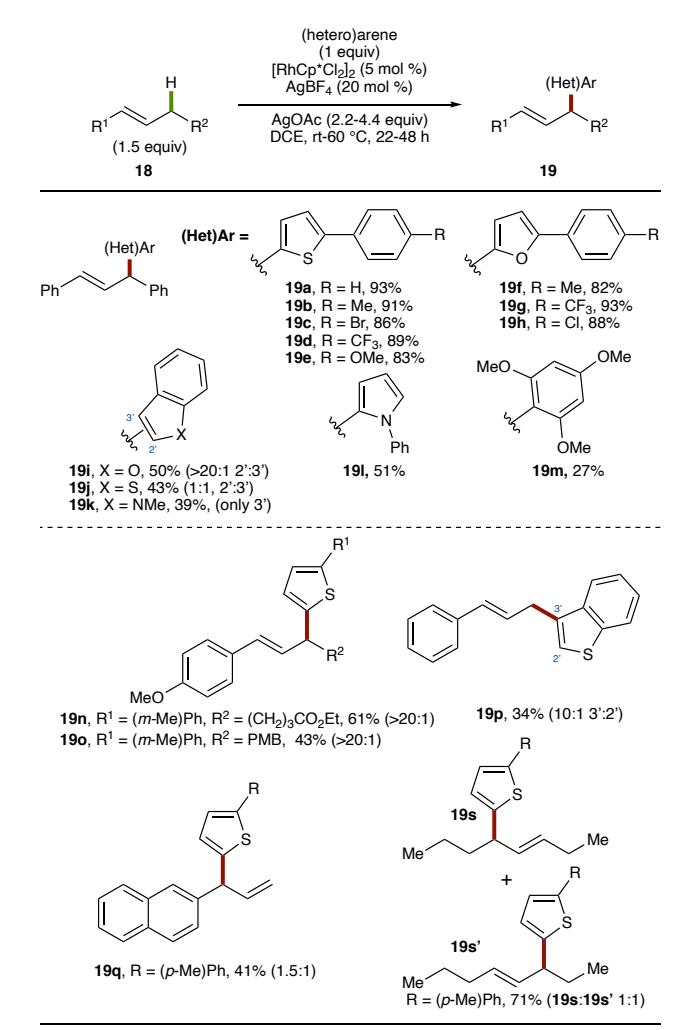


Figure 6: Rh(III)Cp*-catalyzed allylic C-H (hetero)arylation (Glorius, 2018)

In 2019, Glorius and coworkers expanded the scope of RhCp*catalyzed allylic C-H arylation of mono- and disubstituted olefins to include triarylboroxines as the arylating nucleophiles (Figure 7).38 This reaction is proposed to proceed by allylic C-H activation to form the RhCp* $(\pi$ -allyl) complex, followed by transmetalation of the triarylboroxine and subsequent C-C reductive elimination to provide the desired products. Under the reaction conditions, a broad range of electronically diverse triarylboroxines were tolerated, and more electron-rich triarylboroxines delivered the desired products with greater E/Z selectivity (21c and 21d). The authors suggest that this is due to faster transmetalation of the triarylboroxine to the Rh-catalyst, thereby preventing *syn-anti* isomerization of the RhCp*(π -allyl) species leading to greater E-selectivity. However, the regioselectivity drops when the π -allyl intermediate is unsymmetrical. Likewise, the arylation of terminal olefins proceeded in good yields but with poor regioselectivity between the branched and linear arylated products (21e-21g). However, the E/Z selectivity for the linear products arising was consistently >20:1. The reaction occurred selectively at the terminal olefin in the presence of an internal cis olefin (21g). Cyclododecene was also arylated, providing 21h in 44% and 1:1 E/Z selectivity. The allylic arylation of 1,2-disubstituted vinylarenes proceeded with excellent regioselectivity for the linear products in all cases, presumably favoring the products with the olefin in conjugation with the aryl ring (21i-21i).

Mechanistic experiments conducted by the Glorius group indicate that C–H activation is unlikely to be the rate-determining step of this reaction. Additionally, it was demonstrated that in addition to its role as a halide abstractor, AgSbF $_6$ suppresses the competitive homocoupling of the triarylboroxine coupling partners. The authors suggest that the SbF $_6$ counter-anion could do this by decreasing the rate of transmetalation of the triarylboroxine to the rhodium catalyst or accelerating the allylic C–H activation for productive allylic

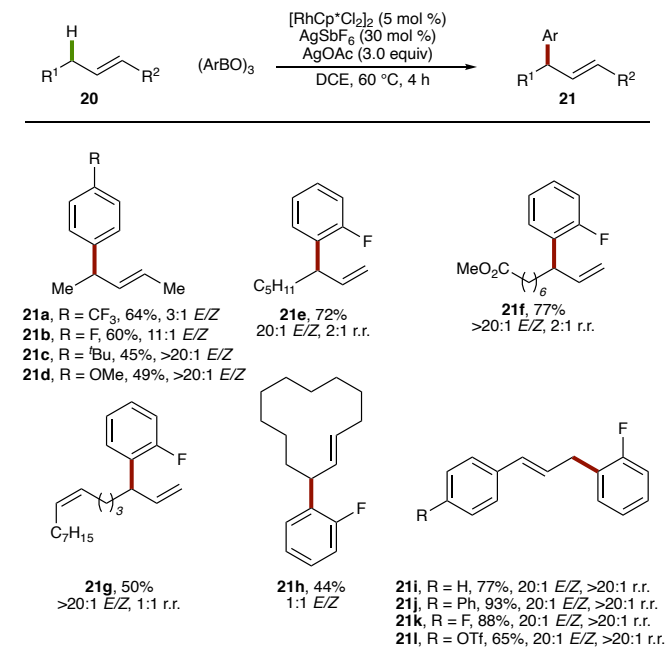


Figure 7: Allylic C-H arylation using triarylboroxines as nucleophiles (Glorius, 2019)

C–H arylation, although no evidence is reported to support this speculation.

Mechanistic investigations

In the intramolecular reaction disclosed by Cossy and coworkers (see Figure 2B),32 it was proposed that the formation of the Rh(III)Cp*(π -allyl) complex was followed by coordination of the nitrogen nucleophile to the metal, and subsequent reductive elimination to form the allylic amine product. The resulting Rh(I)Cp* species could be oxidized to regenerate the Rh(III) intermediate required to cleave the allylic C-H bond and complete the catalytic cycle. However, Tanaka and coworkers showed that a RhCp^E(π -allyl) complex I could be isolated, and was not converted to the allylic amine product until treatment with Cu(OAc)₂·H₂O (see Figure 2C).³³ No experimental evidence to demonstrate if C-X bond formation was occurring via outersphere nucleophilic attack or inner-sphere reductive elimination was presented. In order to design new reactions, and ligands to enhance selectivity in these transformations, a clear understanding of the reaction mechanism was required. In collaboration with MacBeth and Baik, we conducted a series of kinetic, stoichiometric, electrochemical, and computational experiments to elucidate the operative mechanism of the allylic C-H amination.39

In the allylic amination of DPP with benzyl carbamate under standard amination conditions (see Figure 3), a first-order rate dependence on rhodium and olefin concentration was observed. Conversely, the reaction was inversely dependent on the concentration of the carbamate nucleophile. Furthermore, C–H cleavage was shown to be irreversible, with a primary KIE (k_H/k_D) of 2.6, determined by an intermolecular competition kinetic isotope experiment. These data establish that C–H cleavage is the rate-determining step of this reaction.

To shed further light on the key bond forming event, we synthesized a series of stable Rh(III)Cp*(π -allyl) complexes IIIa, IIIb, and IIIc (Figure 8). In particular, the isolation and stability of complexes IIIb and IIIc without any observable formation of the allylic amine 23 or allylic acetate 25, respectively, ruled out both inner-sphere reductive elimination as well as outer-sphere nucleophilic attack as plausible pathways to form 23 or 25 directly from the corresponding Rh(III) complexes. Treatment of complex IIIa with benzyl carbamate and CsOAc did not form any allylic amine 22, instead only yielding $Rh(III)Cp*(\pi-allyl)Cl$ complex IV after a chloride quench (Figure 8A). When the $Rh(III)Cp*(\pi-allyI)(TsNH)$ complex **IIIb** was treated with an oxidant (AgSbF₆) and PhSO₂NH₂ (2 equiv), allylic amines 23 and 24 were observed in a 1:1.5 mixture (10% combined yield, 100% conversion), indicating that neither inner-sphere reductive elimination nor outer-sphere nucleophilic attack to form an allylic amine could be efficiently oxidatively induced (Figure 8B). However, when $Rh(III)Cp^*(\pi-allyI)(OAc)$ complex **IIIc** was treated with AgSbF₆, clean conversion to the allylic acetate 25 was observed in 20 minutes (Figure 8C). These results suggested that an oxidatively induced reductive elimination⁴⁰ of an allylic acetate intermediate was active in the catalytic cycle, with subsequent conversion to the allylic amine product. Density

Figure 8: Stoichiometric studies with Rh(III)Cp*(π -allyI) complexes (Blakey, 2020)

functional theory (DFT) calculations confirmed that reductive elimination of the allylic acetate from Rh(III) to Rh(I) was not feasible with DPP as the substrate and suggested that Rh(IV) \rightarrow Rh(II) reductive elimination was more energetically favorable compared to Rh(V) \rightarrow Rh(III). This was further supported by cyclic voltammetry experiments, which indicated that although Rh(V) was thermodynamically accessible on an electrochemical time scale, Ag⁺ mediated oxidation of Rh(IV) to Rh(V) was unlikely to out-compete reductive elimination from Rh(IV).

The allylic substitution of acetate **26** to the amine **22** was shown to be catalyzed by both Rh(III)Cp* as well as Ag(I) (Figure 9), although time course studies revealed that at 0 °C, the Rh(III)Cp*-catalyzed reaction completed in seconds while the Ag(I)-catalyzed reaction proceeded to completion in 2.5 hours. DFT calculations, indicated that S_N^1 substitution of acetate **26** via an allylic cation was the most feasible mechanism for the Lewis-acid catalyzed allylic substitution.

The mechanism of the silver-promoted allylic C–H amination, determined by experimental, kinetic, electrochemical, and computational analyses, is summarized in Figure 10. The dimeric $[RhCp*Cl_2]_2$ precatalyst is activated by CsOAc and $AgBF_4$ to reveal the cationic complex Va which can be coordinated by the olefin substrate 10e. The following rate-determining concerted-metalation-deprotonation (CMD) step provides $Rh(III)Cp*(\pi-allyI)$ complex Vc. Oxidation of this

Figure 9: Lewis-acid catalyzed allylic amination of acetate 26 (Blakey, 2020)

Figure 10: Proposed mechanism for first-generation allylic amination (Blakey, 2020)

complex to Rh(IV)Cp* and coordination of an acetate anion provides complex Vd, which undergoes C–O reductive elimination to Rh(II)Cp* complex Ve. This then undergoes a second single electron oxidation to regenerate the active catalyst and release the allylic acetate 28, which can undergo a Rh(III)Cp*- or Ag(I)-catalyzed S_N^1 substitution to provide the desired allylic amine product 12e.

Based on the remarkably similar reaction conditions required, as well as the regiochemical outcomes observed in the etherification (see Figure 5)³⁶ and (hetero)arylation (see Figure 6),³⁷ it is likely that these reactions operate under a similar mechanistic paradigm as the allylic amination, i.e. an oxidatively induced reductive elimination of a Rh(IV)Cp*(π -allyl)(OAc) complex, followed by S_N^1 substitution of the allylic acetate with an alcohol or electron-rich aromatic nucleophile, respectively. However, further mechanistic studies are necessary to establish a plausible mechanism for the allylic C–H arylation with triarylboroxine nucleophiles.

On styrenyl substrates, the amination, etherification, and (hetero)arylation reactions were generally selective for the conjugated or linear products over the branched or benzylic isomers. Unfortunately, under this "1st-generation" manifold, C–X bonds were demonstrated to be formed by nucleophilic attack of an allyl cation intermediate, thereby ruling out chiral Rh(III) catalysts to promote enantioselective reactions. These mechanistic insights led us to the hypothesis that reagents containing "internal oxidants", for example a weak N–O bond, that could coordinate the Rh(III)-catalyst and simultaneously oxidize it to Rh(V) would unlock direct reductive elimination as a viable pathway for C–X bond formation.

Allylic Amidation Proceeding *via* Direct C–N Reductive Elimination from M(V) Intermediates

In the allylic amination, etherification, and (hetero)arylation reactions discussed above, the key bond forming steps are postulated to occur by S_N^1 -type allylic substitution of an allylic acetate intermediate, which is the product of an oxidatively induced C–O reductive elimination. In this section, we discuss a new generation of allylic C–H functionalization reactions in which the key C–N bonds are directly formed by inner-sphere reductive elimination, raising the possibility of greater control over regio- and enantioselectivity of C–N bond formation.

Dioxazolones were established as oxidative amidating reagents by Chang and coworkers in the context of directed $C(sp^2)$ –H amidation^{41–46} and have recently been extended to directed $C(sp^3)$ –H amidations as well.^{47–50} These reagents are proposed to oxidize Rh(III)Cp*- and Ir(III)Cp*-complexes to the corresponding M(V)Cp*-nitrenoids, owing to the presence of a cleavable N–O bond which can serve as an internal oxidant. Our group, as well as the groups of Rovis and Glorius, have developed reaction conditions that utilize dioxazolones, and subsequently azides, for the formation of allylic C–N bonds via inner-sphere reductive elimination reactions.

Cp*M(III)-Catalyzed Allylic C-H Amidation

In 2019, we reported the use of dioxazolones for the allylic C–H amidation of unactivated olefins. ⁵¹ With [RhCp*(MeCN)₃](SbF₆)₂ as the catalyst (Figure 11A), a range of alkyl dioxazolones (**31a–31c**) were efficiently coupled with allylbenzene. Cyclic ethers (**31d**) and sulfones (**31e**), as well as *N*-Boc piperidine (**31f**) were also good reaction partners. These reactions were high yielding, and were generally selective for the branched amide products, in sharp contrast to our 1st generation amination reaction. For terminal olefins with low yields and poor selectivity under Rhcatalysis, the use of [IrCp*Cl₂]₂ as the precatalyst was critical to restore reactivity and high levels of regioselectivity for the branched amide product (**31h–31j**).

This was consistent with the reports of Ir-catalyzed allylic C–H amidation that were simultaneously and independently published by the Rovis and Glorius groups (Figure 11B and 11C).^{52,53} These reactions demonstrated excellent functional group compatibility across a range of diversely substituted terminal olefins and dioxazolones. Notably, alkyl bromides (31m) and cyanides (31n) were well tolerated, as well as a thiophene-derived dioxazolone (31y). In all three reports, the reaction benefitted from having a slight excess of Ag(I) in solution, in addition to the silver required for halide abstraction from the dimeric precatalysts. The role of Ag(I) is still unclear, although Rovis and coworkers suggest that AgNTf₂ helps with the dissociation of the acetate ligand or amide products from iridium and prevents catalyst arrest.

In the allylic C–H amidation of 1,2-disubstituted vinylarenes, we observed complementary reactivity between RhCp* and IrCp* catalysts (Figure 12). For example, using RhCp* as the

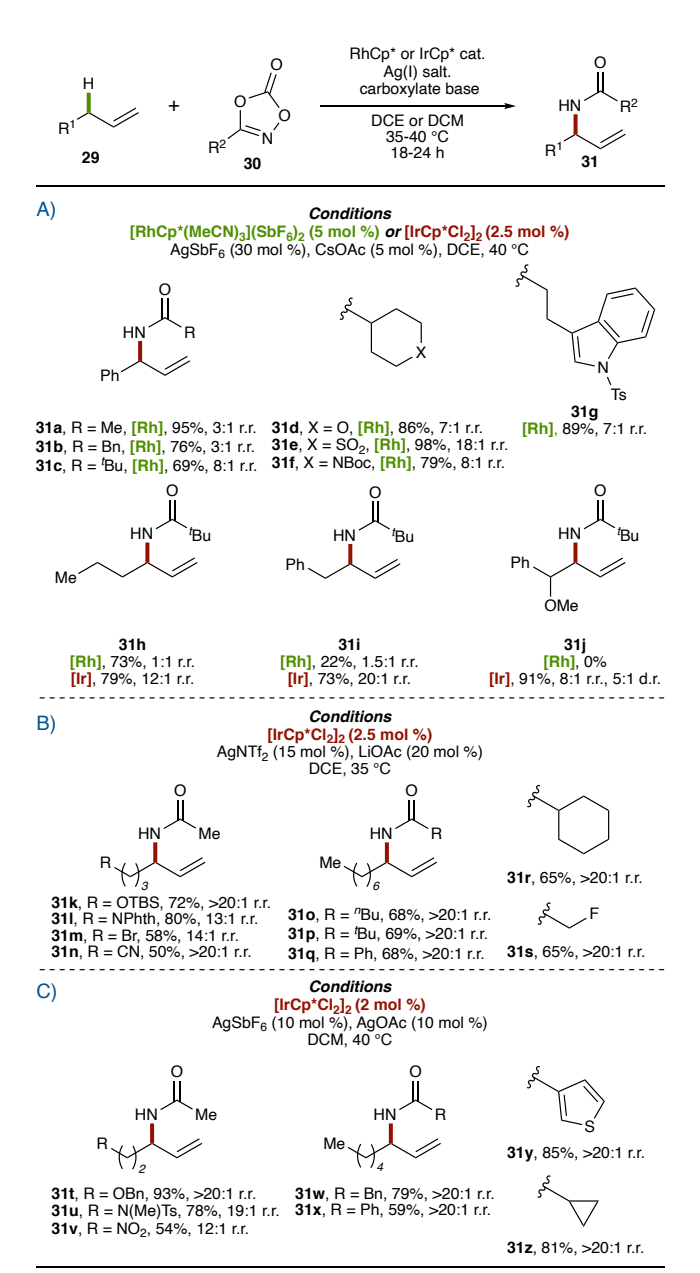


Figure 11: Allylic C–H amidation with dioxazolones. A) Blakey, 2019, B) Rovis, 2019, C) Glorius, 2019

Figure 12: Complementary regioselectivity of 1,2-disubstituted vinylarenes with RhCp* and IrCp* catalysts

catalyst provided pivalamide **33a** in 78% yield with 16:1 regioselectivity for the benzylic amide isomer. However, when IrCp* was used, the yield was reduced to 45% and regioselectivity was overturned to favor the conjugated amide product **34a** (1:7 r.r.). Likewise, amide product **33b** could be isolated in 86% yield and >20:1 regioselectivity for the benzylic isomer under RhCp* catalysis, but the yield (39%) and regioselectivity (7:1 r.r.) were reduced when IrCp* was used. A similar trend was observed in the amidation of a phenylalanine-derived disubstituted olefin (**33c**).

Our group, as well as the Rovis group, have also demonstrated that tosyl azide is also an effective nitrenoid precursor for allylic C–H sulfamidation (Figure 13).^{52,54} Under two different sets of conditions, a wide range of terminal olefins could be sulfamidated with excellent selectivity for the branched position (>20:1 r.r. in all cases). The substrate scope includes unactivated olefins (36a and 36b) and a wide range of allylbenzene derivatives (36c–36h).

Mechanistic Investigations

The mechanism of the allylic C-H amidation with dioxazolones has been investigated using kinetic and stoichiometric experiments. Allylic C-H cleavage was shown to be irreversible by Rovis and coworkers;52 no deuterium exchange was observed when deuterated substrate 37-d2 was amidated at the allylic position in the presence of acetic acid under standard conditions (Figure 14A). Additionally, demonstrated that RhCp*- and IrCp*(π-allyl)Cl complexes IV-Rh and IV-Ir were quickly converted to the corresponding pivalamide products 39 and 40 when treated with tert-butyl dioxazolone and AgSbF₆, with regiochemical ratios that were consistent with the catalytic reactions (Figure 14B).51 Rovis and coworkers also reported the stoichiometric conversion of an

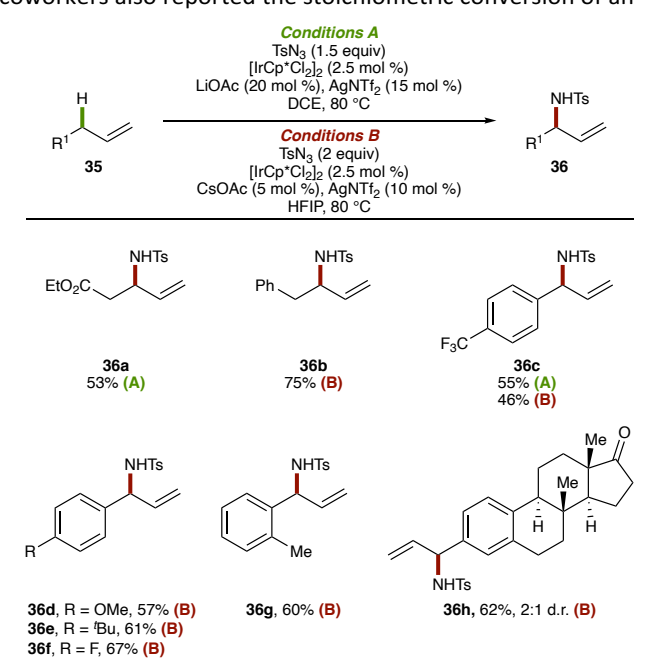


Figure 13: Allylic C–H sulfamidation with TsN₃. Conditions A) Blakey, 2019, Conditions B) Rovis, 2019

NHPIv

A. Deuterium exchange studies

B. Stoichiometric studies

Figure 14: Mechanistic investigation of allylic C–H amidation with dioxazolones $IrCp^*(\pi-allyl)$ complex to its allylic amide product.⁵² These stoichiometric studies, together with the regioconvergent allylic amidation of olefin isomers reported by Glorius and coworkers,⁵³ and the regioisomeric products obtained when the reaction is performed on 1,2-disubstituted olefins indicate that these reactions proceed through MCp*(π -allyl) complexes.

Based on these studies, the following catalytic cycle for allylic C–H amidation has been proposed (Figure 15). The allylic sulfamidation (see Figure 13) also likely proceeds through a similar mechanism. The precatalyst is activated by a halide scavenger and coordinated by acetate to form the active catalyst **VIa**. Following olefin coordination, complex **VIb** undergoes irreversible concerted metalation deprotonation (CMD) to form coordinatively unsaturated cationic complex **VIc**.

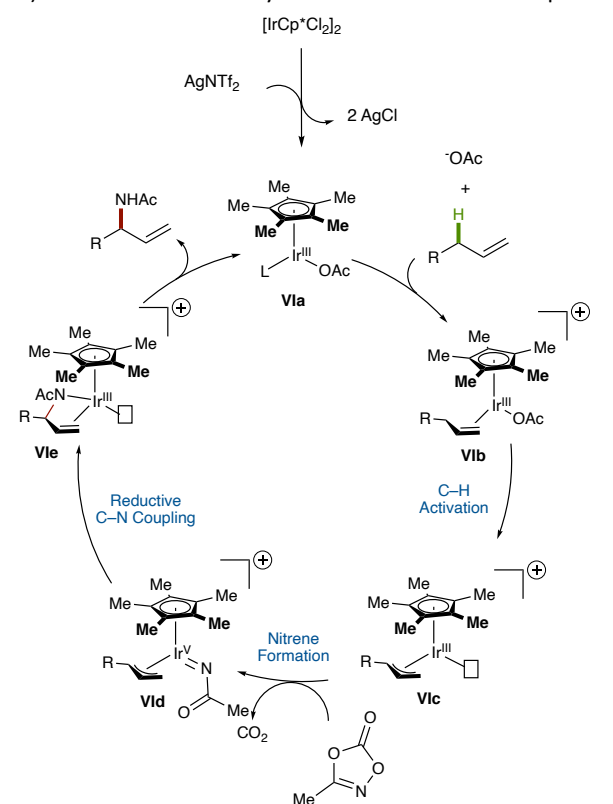


Figure 15: Proposed catalytic cycle for allylic C–H amidation via M(V)(π -allyl) nitrenoid intermediates

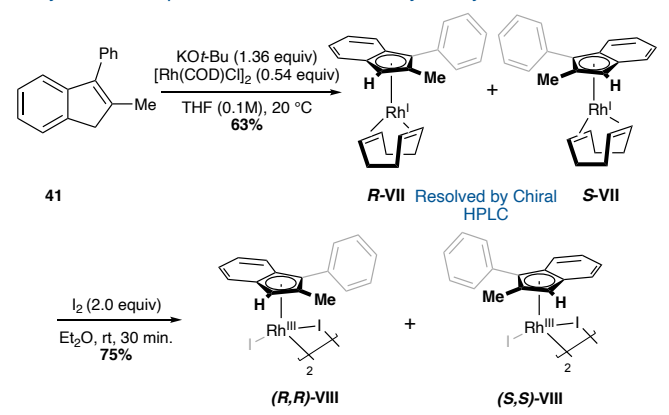
The dioxazolone can then coordinate and release CO_2 to form nitrenoid complex **VId**, which undergoes C–N reductive coupling to form complex **VIe**. Protodemetalation then releases the amide product and regenerates the active catalyst.

Designer Ligands for Selective C-H Amidation

With a reasonable understanding of a new mechanism for oxidatively induced allylic C–H functionalization in which the key bond forming event is ostensibly an inner-sphere reductive elimination, we set out to develop an easily accessible, modular, and broadly applicable catalyst system for enantioselective transformations. In 2020, in collaboration with the Baik group, we reported the development of a new class of planar chiral rhodium indenyl catalyst and demonstrated its application to enantioselective allylic C–H amidation.⁵⁵ The dimeric precatalyst was prepared by complexing 2-methyl-3-phenylindene (41) with [Rh(I)(COD)Cl]₂ to provide complex VII (Figure 16A). The enantiomers of this planar chiral complex could then be resolved by chiral HPLC and oxidized with I₂ to provide each enantiomer of the desired diiodide precatalyst (VIII).

The indenyl ligand, which is known to coordinate along a continuum between η^{5-} and η^{3-} -coordination modes, is postulated to induce an electronic asymmetry in complexes such as π -allyl complex **(S)-IX**, obtained from precatalyst **(S,S)-VIII** and 2-pentene (Figure 16B).^{56,57} As depicted, the Rh–C20 bond *trans* to C1-C5-C4 of the indenyl ligand is longer than the Rh–C18 bond *trans* to C2-C3 (Rh–C20 = 2.2196 Å and Rh–C18 = 2.1457 Å). This is indicative of the differing *trans* effects exerted by the two sides of the indenyl ligand on a symmetrical π -allyl fragment as a result of the asymmetry induced by the indenyl effect.^{58–61}

A. Synthesis of a planar chiral rhodium indenyl catalyst



B. The indenyl effect in a rhodium indenyl π -allyl complex

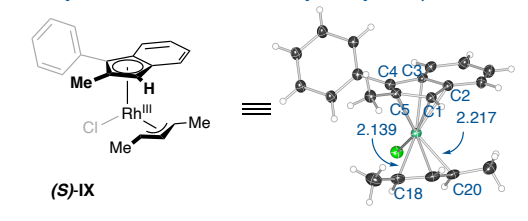


Figure 16: A planar chiral rhodium indenyl catalyst for enantioselective allylic C–H functionalization (Blakey, 2020)

The allylic amidation worked well across a broad range of dioxazolone and olefin substrates (Figure 17). For terminal olefins, the reaction was selective for branched amide products. Methyl- (43a), tert-butyl- (43b), and cyclohexyl-dioxazolone (43c) were all suitable substrates, as well as glycine-derived dioxazolone (43d). Simple, unactivated olefins were also effective coupling partners, delivering the olefin products 43e and 43f in high yields and enantioselectivities. Internal olefins were also reactive (43g and 43h), as well as a substrate containing a homo-allylic methyl substituent, which produced amide product 43i with excellent diastereoselectivity. We observed that more Lewis basic dioxazolones performed better at lower temperatures. We speculated that these dioxazolones could competitively coordinate the catalyst before C-H activation to form the key π -allyl complex, leading to deleterious side reaction pathways.

This putative mechanism for this reaction is similar to the proposed mechanism for the racemic allylic amidation shown above (see Figure 15). Computational studies indicate that C–H cleavage to form the $\pi\text{-allyl}$ complex is rate- and enantio-determining, and the stereochemical information set at this stage is preserved through the subsequent steps of the reaction. C–N reductive elimination from the Rh(V)-nitrenoid intermediate was calculated to be regio-determining.

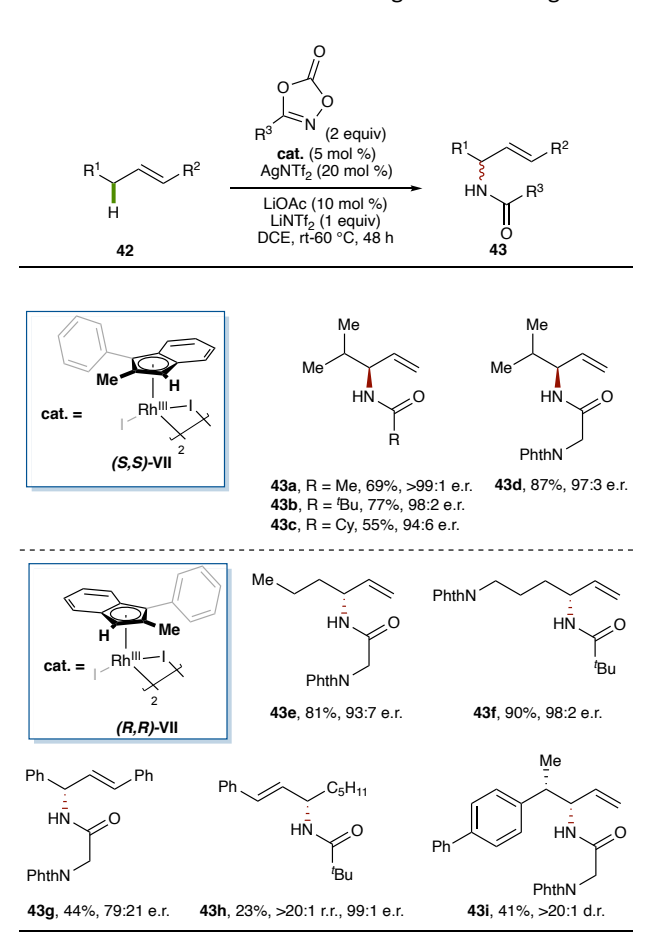


Figure 17: Enantioselective C–H amidation with a planar chiral rhodium indenyl catalyst (Blakey, 2020)

In 2020, Rovis and coworkers expanded on this mechanistic paradigm and reported the development of catalysts for the remarkably regioselective C-H activation and sulfamidation of 1,1- and trans-1,2-disubstituted alkenes containing nearly identical allylic C-H bonds.⁶² Using the slightly less bulky $[IrCp^{TM}Cl_2]_2$ (Cp^{TM} = tetramethylcyclopentadienyl) as the precatalyst and TsN3 as the nitrenoid precursor, several 1,1disubstituted olefins containing an electron-withdrawing substituent were sulfamidated at the allylic position (Figure 18A). In almost all cases, the reaction was selective for the allylic position distal from the electron-withdrawing group (EWG). However, this regioselectivity decreased as the EWG was moved further away from the allylic position, presumably due to the decreased inductive influence of the substituent (45a-45f). The inductive effect had a similar influence on regioselectivity in substrates containing electronically diverse homoallylic aryl substituents (45g-45i). In contrast, the opposite regioselectivity was observed when the distal allylic position was a methyl group (46j and 46k), i.e. the reaction was selective for methylene C-H bonds over methyl C-H bonds, and this selectivity was exacerbated when the EWG was moved further away. The authors demonstrated that this inductive influence on the regioselectivity of allylic C-H sulfamidation is directly correlated with the ¹J_{CH} coupling constants of the allylic C–H bonds (Figure 18B). Thus, as the CF₃ group is moved further away from the olefin, $\Delta^1 J_{CH}$ decreases and the regioselectivity for the distal allylic position (with the smaller ¹J_{CH}) is diminished.

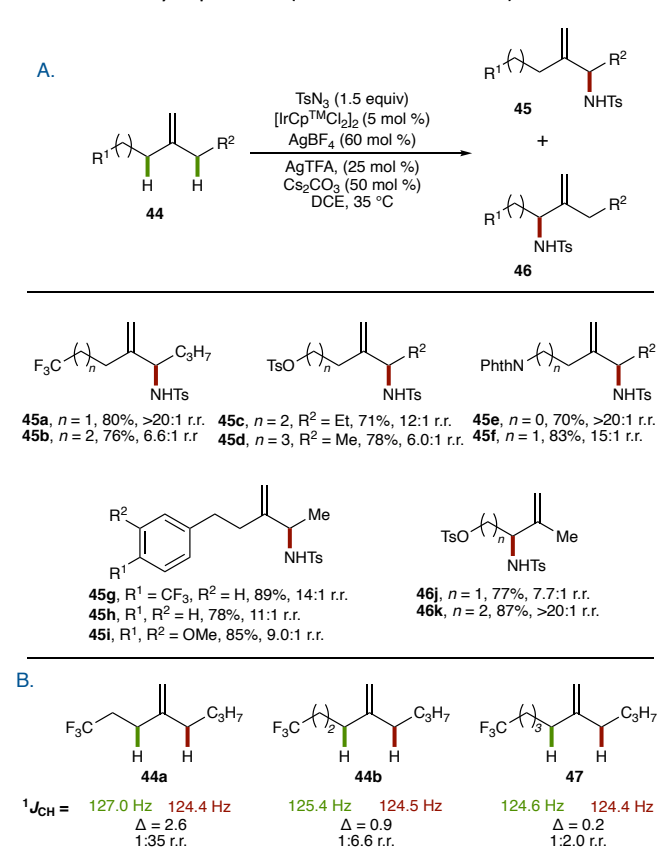


Figure 18: A) Regioselective sulfamidation of 1,1-disubstituted olefins with distal electron-withdrawing substituents, B) Regioselectivity is correlated with $\Delta^{1}J_{CH}$ (Rovis, 2020)

In the same report, Rovis and coworkers investigated the regioselectivity of allylic C-H amidation of 1,2-disubstituted olefins (Figure 19). The same inductive influence of the EWG was observed, and C-H activation occurred selectively at the allylic position distal from the tosylate group. Only the allylic functionalization products (49 and 50) arising from distal C-H activation were observed. With a broad range of IrCp precatalyst derivatives, it was observed that regioselectivity of the amidation improved as substituents were removed from the Cp ligand (Xa-Xc). Once the monosubstituted Cp ring had been established as having the optimal steric environment for selectivity, additional electronic tuning, in which a silyl substituent on the methyl-Cp ligand was introduced (Xd), improved the yield of the reaction (79%). This ligand was designed to maintain minimal steric encumbrance, but to increase the electron density on the Cp ligand through the hyperconjugative electron-donating effect of the pendent silane.

Co-Catalyzed Allylic C-H Functionalization

Although CoCp*-complexes have seen widespread use in catalytic C(sp²)-H activation, no examples of CoCp*-catalyzed allylic C-H functionalization have been reported. 63-66 Cobalt complexes display more nucleophilic character than the rhodium and iridium organometallic intermediates discussed thus far, due to the lower electronegativity of Co as compared to Rh, Ir. Taking advantage of this reactivity, in 2017, Sato and co-workers reported the cobalt catalyzed carboxylation of allylic C-H bonds with CO₂ (Figure 20).⁶⁷ Under a Co(acac)₂ (10 mol %) and Xantphos (20 mol %) catalyst system, a wide range of allybenzene derivatives were carboxylated at the linear position. The yield of the carboxylic acid product decreased as electron-density in the aryl decreased (52a-52f). Substrates with carbonyl-containing functional groups like esters (52d) or amides (52e) were well tolerated, as well as heteroaromatic rings (52f). The reaction worked well on diene substrates (52g, 78% yield). In almost all cases, the linear carboxylated products were isolated selectively. In contrast, when performed on alkyl olefin 51h, however, a mixture of isomers 52h, 52h', and 52h" was isolated in 24% yield.

A simplified catalytic cycle for this reaction is depicted in Figure

Figure 19: Steric effect of the Cp ligand on regioselective allylic C–H amidation of 1,2-disubstituted olefins (Rovis, 2020)

$$R = \begin{array}{c} Co(acac)_2 \ (10 \ mol \ \%) \\ Xantphos \ (20 \ mol \ \%) \\ AlMe_3 \ (1.5-2 \ equiv) \\ \hline DMA, 60 ^{\circ}C \\ CsF \ (1 \ equiv), CO_2 \ (1 \ atm, \ closed) \\ 12-16 \ h \\ \hline \\ R = \begin{array}{c} OMe \\ 52a, 81\% \\ \hline \\ 52b, R = Ph, 71\% \\ \hline \\ 52c, R = CF_3, 65\% \\ \hline \\ 52d, R = CO_2Me, 63\% \\ \hline \\ 52e, R = Bz, 77\% \\ \hline \\ CO_2H \\ CO_2H \\ \hline \\ CO_2H \\$$

Figure 20: Co-catalyzed allylic C-H carboxylation with CO₂ (Sato, 2017)

21. The authors observed that Co(I), Co(II), and Co(III) complexes were all effective catalysts for this carboxylation reaction. Therefore, Co(I) complex **XIa** was hypothesized to be the active catalyst in the reaction, produced by disproportionation of Co(II) and reductive elimination of Co(III). Olefin coordination and C–H activation would then provide Co(III)(π -allyl) complex **XIc**. Xantphos assisted tautomerization to form η^1 -allyl Co(III) species **XId** and reductive elimination of methane would form nucleophilic η^1 -allyl Co(I) complex **XIe**. Carboxylation would then provide **XIf** which would transmetallate with AlMe₃ to form the aluminate **XIg** and regenerate the active Co(I) catalyst. The authors hypothesize that the increased yield observed in the presence of CsF is due to the resulting increased solubility of CO₂.

In a subsequent report, Sato and co-workers extended this mechanistic paradigm to include electrophilic ketones to generate homoallylic tertiary alcohol products (Figure 22).⁶⁸ Under these remarkably similar reaction conditions, a wide range of ketones were compatible reaction partners. The authors observed that selectivity for the linear ketone product increased with steric bulk around the ketone (54a-54c). Furthermore, addition to acetophenone 54e with

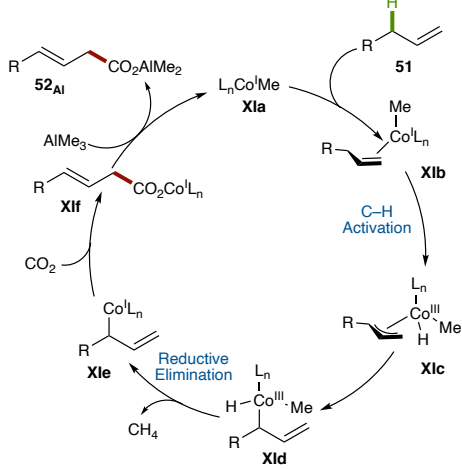


Figure 21: Proposed catalytic cycle for Co-catalyzed allylic C-H carboxylation (Sato, 2017)

Figure 22: Co-catalyzed addition of C(sp3)-H bonds to ketones (Sato, 2017)

a more electron-rich aryl ring resulted in exclusive formation of the linear product. The authors correlated this with the carbonyl bond strengths as depicted by the C=O stretching frequencies (54d = 1694 cm⁻¹, 54e = 1675 cm⁻¹). A similar trend was observed with cyclic ketones; as the C=O bond strength decreased with expanding ring-size (54f = 1783 cm⁻¹, 54g = 1715 cm⁻¹, 54h = 1701 cm⁻¹), selectivity for the linear product was exacerbated.

Cascade Reactions Involving Allylic C-H Functionalization

In addition to several recent advances to Rh- and $Ir(\pi-allyl)$ chemistry, there have also been key reports in the development of cascade reactions involving mechanistically distinct pathways of allylic C–H functionalization. Selected examples, involving alkyne coupling partners, are discussed here.

In 2015, Rovis and coworkers reported the formation of azabicycles through Rh(III)Cp*-catalyzed allylic C-H activation of alkenyl sulfonamides in the presence of diarylalkynes (Figure 23).⁶⁹ Azabicycles of increasing ring sizes were accessible (58a-58c) and symmetrical electron-rich alkynes also reacted favorably (58d-58f). The authors' proposed mechanism begins with activation of the allylic C-H bond of 56a to form Rh(III)Cp*(π -allyl) complex **XIIa** in equilibrium with the η^1 complex XIIb. Migratory insertion of diphenylacetylene and subsequent 1,3-Rh migration provides complex XIIc which could undergo a 4π -conrotatory electrocyclization *via* complex **XIId** to provide \(\eta^3\)-complex **XIIe**. The excellent diastereoselectivity observed in these reactions is attributed to this step. The authors speculated that the allylic C-N bond is formed via an inner-sphere reductive elimination from Rh(III)Cp*-complex XIIf, and the resulting Rh(I) complex could be oxidized to regenerate the active Rh(III) catalyst.

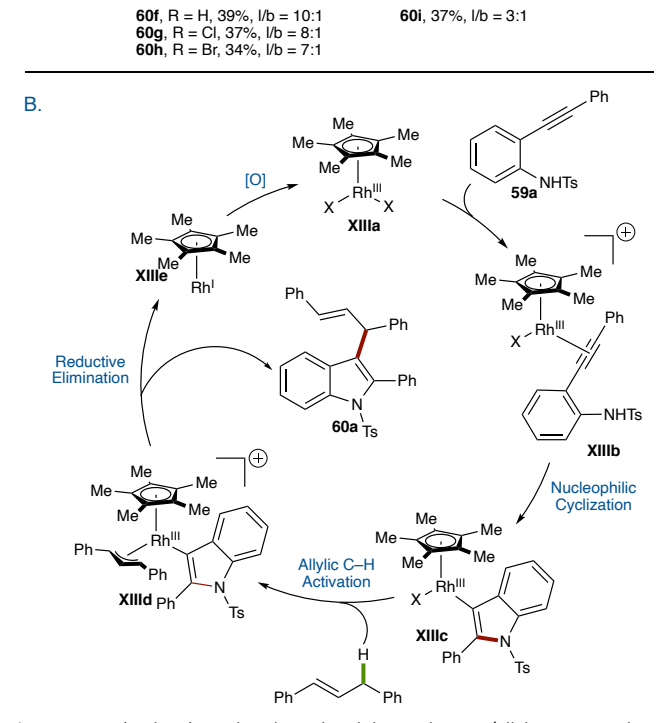
In 2019, Li and coworkers described a nucleophilic cyclization/allylic C–H arylation sequence for the synthesis of C3-allylated/C2-substituted indoles from o-alkynylanilines (Figure 24A). The reaction was effective across a broad range of electronically diverse aryl alkynes delivering the disubstituted indoles in good yields (**60a–60d**), with DPP as the allyl coupling partner. Reaction with 4-octene delivered a 1:1 mixture of regioisomeric products **60e** and **60e'** in 40% yield, supporting the intermediacy of a Rh(III)Cp*(π -allyl) complex in the catalytic

Figure 23: A) Synthesis of azabicycles via RhCp*-catalyzed allylic C–H amination, B) Proposed catalytic cycle (Rovis, 2015) cycle. Notably, in the case of terminal π -allyl complexes, the

linear products were favored over the branched (60f–60i), which is consistent with the regioselectivity observed in (hetero)arylation disclosed by Glorius et al. However, *N*-Ts-2-

Ph-indole was an ineffective nucleophile in the direct allylic C–H arylation of DPP, suggesting that the allylation process shown here is mechanistically distinct from the 1st generation protocol outlined above for the amination, etherification, and arylation reactions. In the proposed catalytic cycle (Figure 24B), the oalkynylaniline **59a** can coordinate an activated Rh(III)Cp* catalyst **XIIIa** to form cationic complex **XIIIb** which can undergo nucleophilic cyclization with the pendant tosylamide to form complex **XIIIc**. Allylic C–H activation of the olefin leads to Rh(III)Cp*(π -allyl) complex **XIIId**. At this stage, reductive elimination provides the indole product **60a** and oxidation of the resulting Rh(I)Cp* complex **XIIIe** regenerates the active catalyst.

In both of the examples presented here from the Rovis (Figure 23) and Li (Figure 24) groups, it is unclear whether the key bond forming steps occur via reductive elimination from Rh(III)Cp* – as proposed by the authors – or are oxidatively induced to occur from higher oxidation RhCp* species, as shown in the $1^{\rm st}$ and $2^{\rm nd}$ generation allylic C–H functionalization reactions presented above.



60i, 37%, I/b = 3:1

Figure 24: A) RhCp*-catalyzed nucleophilic cyclization/allylic C-H arylation cascade reaction, B) Proposed catalytic cycle (Li, 2019)

Conclusions

Rh(III)- and Ir(III)-catalyzed allylic C-H functionalization has rapidly emerged as an enabling technology for the atom- and step-economical modification of both feedstock olefins and more complex substrates. Early insights from Li, Cossy, and Tanaka demonstrated the suitability of RhCpx catalysts for intramolecular allylic C-H amination with an enhanced scope of nitrogen nucleophiles. This manifold has since been expanded upon with contributions to intermolecular transformations from our group, the Rovis group, and the Glorius group, among others.

Two distinct mechanistic pathways for allylic C-H functionalization have been established: 1) reactions proceeding by oxidatively induced reductive elimination of an allylic acetate in the presence of an external stoichiometric oxidant followed by S_N¹ substitution with a nitrogen (e.g. Cbz(Me)NH₂), oxygen (e.g. ROH), or carbon-based (e.g. heteroaryl) nucleophile, and 2) direct C-N reductive coupling from a Rh(V)- or Ir(V)-nitrenoid complex. In particular, the allylic C–H amidation has served as a proving ground for new catalyst systems. We reported the development of a class of modular and easily accessible planar chiral indenyl complexes for enantioselective allylic C-H amidation. Rovis and coworkers described the predictive value of ¹J_{CH} coupling constants for site-selective C-H activation and reported a new catalyst for regioselective allylic C-H amidation. However, while significant advances have been made in this research area, some limitations remain.

While the operative mechanisms for 1st-generation allylic amination, etherification, and heteroarylation, and 2ndgeneration amidation and sulfamidation are established and supported by experimental and computational data, further studies are necessary to elucidate a plausible mechanism for the allylic C-H arylation with triarylboroxine nucleophiles.

In line with the growing importance of sustainable practices in organic chemistry, we expect that future work in this arena will be directed towards the development of earth-abundant metal catalyzed transformations. Compared to Rh- and Ircatalysis, Co-catalyzed allylic C–H functionalization is a relatively unexplored area of catalysis, with the exception of the allylic C-H carboxylation and alkenylation via low-valent nucleophilic $Co(\pi-allyl)$ complexes discussed above. Furthermore, excluding the 2nd-generation allylic amidation reports, the current Rh- and Ir-catalyzed allylic C–H functionalization literature relies on stoichiometric Agi oxidants for catalyst turnover, severely hampering its applicability and scalability. We envision significant room for future reaction and catalyst development in all these areas.

Conflicts of interest

There are no conflicts to declare.

Acknowledgements

This work was supported by the National Science Foundation (NSF) under the CCI Center for Selective C-H Functionalization (CHE-1700982), and the American Chemical Society Petroleum Research Fund (ACS-PRF-59563-ND1).

Notes and references

- L. McMurray, F. O'Hara and M. J. Gaunt, Chem. Soc. Rev., 2011, 40, 1885-98.
- M. Lafrance, N. Blaquiere and K. Fagnou, Eur. J. Org. Chem.,

- 2007, **2007**, 811–825.
- 3 D. A. Colby, R. G. Bergman and J. A. Ellman, *Chem. Rev.*, 2010, **110**, 624–655.
- 4 H. M. L. Davies and Y. Lian, *Acc. Chem. Res.*, 2012, **45**, 923–935.
- J. Yamaguchi, A. D. Yamaguchi and K. Itami, *Angew. Chem. Int. Ed.*, 2012, **51**, 8960–9009.
- 6 K. Godula, Science, 2006, **312**, 67–72.
- J. Ye and M. Lautens, *Nat. Chem.*, 2015, **7**, 863–870.
- A. F. M. Noisier and M. A. Brimble, *Chem. Rev.*, 2014, **114**, 8775–8806.
- 9 R. Manoharan and M. Jeganmohan, *Eur. J. Org. Chem.*, 2020, doi.org/10/1002/ejoc.202000936.
- T. A. F. Nelson, M. R. Hollerbach and S. B. Blakey, *Dalt. Trans.*, DOI:10.1039/D0DT02313B.
- Q. Cheng, H.-F. Tu, C. Zheng, J.-P. Qu, G. Helmchen and S.-L. You, *Chem. Rev.*, 2019, **119**, 1855–1969.
- N. A. Butt and W. Zhang, Chem. Soc. Rev., 2015, 44, 7929–7967.
- B. M. Trost and M. L. Crawley, Chem. Rev., 2003, 103, 2921–2944.
- J. Qu and G. Helmchen, Acc. Chem. Res., 2017, 50, 2539–
 2555.
- B. W. H. Turnbull and P. A. Evans, J. Org. Chem., 2018, 83, 11463–11479.
- 16 M. S. Chen and M. C. White, J. Am. Chem. Soc., 2004, 126, 1346–1347.
- 17 M. S. Chen, N. Prabagaran, N. A. Labenz and M. C. White, *J. Am. Chem. Soc.*, 2005, **127**, 6970–6971.
- T. J. Osberger and M. C. White, J. Am. Chem. Soc., 2014,
 136, 11176–11181.
- S. E. Ammann, W. Liu and M. C. White, *Angew. Chem. Int. Ed.*, 2016, **55**, 9571–9575.
- 20 C. C. Pattillo, I. I. Strambeanu, P. Calleja, N. A. Vermeulen, T. Mizuno and M. C. White, *J. Am. Chem. Soc.*, 2016, **138**, 1265–1272.
- 21 K. J. Fraunhoffer and M. C. White, *J. Am. Chem. Soc.*, 2007, **129**, 7274–7276.
- D. J. Covell and M. C. White, *Angew. Chem. Int. Ed.*, 2008,
 47, 6448–6451.
- S. A. Reed and M. C. White, J. Am. Chem. Soc., 2008, 130, 3316–3318.
- 24 A. J. Young and M. C. White, J. Am. Chem. Soc., 2008, 130, 14090–14091.
- 25 S. A. Reed, A. R. Mazzotti and M. C. White, *J. Am. Chem. Soc.*, 2009, **131**, 11701–11706.
- N. A. Vermeulen, J. H. Delcamp and M. C. White, J. Am. Chem. Soc., 2010, 132, 11323–11328.
- I. I. Strambeanu and M. C. White, J. Am. Chem. Soc., 2013, 135, 12032–12037.
- S. E. Ammann, G. T. Rice and M. C. White, *J. Am. Chem. Soc.*, 2014, 136, 10834–10837.
- 29 R. Wang, Y. Luan and M. Ye, *Chin. J. Chem.*, 2019, **37**, 720–
- 30 R. A. Fernandes and J. L. Nallasivam, *Org. Biomol. Chem.*, 2019, 17, 8647–8672.
- 31 X. Li, X. Gong, M. Zhao, G. Song, J. Deng and X. Li, *Org.*

- Lett., 2011, 13, 5808-5811.
- T. Cochet, V. Bellosta, D. Roche, J. Y. Ortholand, A. Greiner and J. Cossy, *Chem. Commun.*, 2012, 48, 10745–10747.
- 33 Y. Shibata, E. Kudo, H. Sugiyama, H. Uekusa and K. Tanaka, *Organometallics*, 2016, **35**, 1547–1552.
- J. S. Burman and S. B. Blakey, *Angew. Chem. Int. Ed.*, 2017,56, 13666–13669.
- 35 P. Sihag and M. Jeganmohan, *J. Org. Chem.*, 2019, **84**, 13053–13064.
- 36 T. A. F. Nelson and S. B. Blakey, *Angew. Chem. Int. Ed.*, 2018, **57**, 14911–14915.
- A. Lerchen, T. Knecht, M. Koy, J. B. Ernst, K. Bergander, C.
 G. Daniliuc and F. Glorius, *Angew. Chem. Int. Ed.*, 2018, 57, 15248–15252.
- T. Knecht, T. Pinkert, T. Dalton, A. Lerchen and F. Glorius, ACS Catal., 2019, 9, 1253–1257.
- 39 R. J. Harris, J. Park, T. A. F. Nelson, N. Iqbal, D. C. Salgueiro, J. Bacsa, C. E. Macbeth, M. H. Baik and S. B. Blakey, *J. Am. Chem. Soc.*, 2020, **142**, 5842–5851.
- K. Shin, Y. Park, M. H. Baik and S. Chang, *Nat. Chem.*, 2018,
 10, 218–224.
- 41 J. Park, J. Lee and S. Chang, *Angew. Chem. Int. Ed.*, 2017, **56**, 4256–4260.
- 42 Q. A. Chen, Z. Chen and V. M. Dong, *J. Am. Chem. Soc.*, 2015, **137**, 8392–8395.
- 43 Y. Park, J. Heo, M.-H. Baik and S. Chang, *J. Am. Chem. Soc.*, 2016, **138**, 14020–14029.
- 44 Y. Hwang, Y. Park and S. Chang, *Chem. Eur. J.*, 2017, **23**, 11147–11152.
- 45 Y. Park, S. Jee, J. G. Kim and S. Chang, *Org. Process Res. Dev.*, 2015, **19**, 1024–1029.
- 46 J. Park and S. Chang, Angew. Chem. Int. Ed., 2015, 54, 14103–14107.
- P. W. Tan, A. M. Mak, M. B. Sullivan, D. J. Dixon and J.
 Seayad, Angew. Chem. Int. Ed., 2017, 56, 16550–16554.
- 48 H. Shi and D. J. Dixon, *Chem. Sci.*, 2019, **10**, 3733–3737.
- 49 H. Wang, Y. Park, Z. Bai, S. Chang, G. He and G. Chen, *J. Am. Chem. Soc.*, 2019, **141**, 7194–7201.
- 50 S. Y. Hong, Y. Park, Y. Hwang, Y. B. Kim, M.-H. Baik and S. Chang, *Science*, 2018, **359**, 1016–1021.
- 51 J. S. Burman, R. J. Harris, C. M. B. Farr, J. Bacsa and S. B. Blakey, ACS Catal., 2019, 9, 5474–5479.
- 52 H. Lei and T. Rovis, *J. Am. Chem. Soc.*, 2019, **141**, 2268–2273.
- T. Knecht, S. Mondal, J.-H. Ye, M. Das and F. Glorius, *Angew. Chem. Int. Ed.*, 2019, **58**, 7117–7121.
- A. M. Kazerouni, T. A. F. Nelson, S. W. Chen, K. R. Sharp and
 S. B. Blakey, J. Org. Chem., 2019, 84, 13179–13185.
- C. M. B. Farr, A. M. Kazerouni, B. Park, C. D. Poff, J. Won, K.
 R. Sharp, M.-H. Baik and S. B. Blakey, *J. Am. Chem. Soc.*,
 2020, 142, 13996–14004.
- 56 M. E. Rerek, L. N. Ji and F. Basolo, J. Chem. Soc. Chem. Commun., 1983, 1208–1209.
- M. E. Rerek and F. Basolo, *Organometallics*, 1983, 2, 372–376.
- T. B. Marder, J. C. Calabrese, D. C. Roe and T. H. Tulip, Organometallics, 1987, 6, 2012–2014.

- 59 A. J. Hart-Davis and R. J. Mawby, *J. Chem. Soc. A Inorganic, Phys. Theor. Chem.*, 1969, **0**, 2403–2407.
- S. A. Westcott, A. K. Kakkar, G. Stringer, N. J. Taylor and T.
 B. Marder, J. Organomet. Chem., 1990, 394, 777–794.
- B. M. Trost and M. C. Ryan, *Angew. Chem. Int. Ed.*, 2017,56, 2862–2879.
- 62 H. Lei and T. Rovis, *Nat. Chem.*, 2020, **12**, 725–731.
- 63 M. Moselage, J. Li and L. Ackermann, *ACS Catal.*, 2016, **6**, 498–525.
- 64 S. M. Ujwaldev, N. A. Harry, M. A. Divakar and G. Anilkumar, *Catal. Sci. Technol.*, 2018, 8, 5983–6018.
- A. Baccalini, S. Vergura, P. Dolui, G. Zanoni and D. Maiti, Org. Biomol. Chem., 2019, 17, 10119–10141.
- 66 T. Yoshino and S. Matsunaga, *Asian J. Org. Chem.*, 2018, **7**, 1193–1205.
- K. Michigami, T. Mita and Y. Sato, *J. Am. Chem. Soc.*, 2017, 139, 6094–6097.
- T. Mita, S. Hanagata, K. Michigami and Y. Sato, *Org. Lett.*,2017, 19, 5876–5879.
- A. Archambeau and T. Rovis, *Angew. Chem. Int. Ed.*, 2015,54, 13337–13340.
- J. Sun, K. Wang, P. Wang, G. Zheng and X. Li, *Org. Lett.*,2019, **21**, 4662–4666.